

Broadband perfect absorber based on one ultrathin layer of refractory metal

Huixu Deng,^{1,†} Zhigang Li,^{1,†} Liliana Stan,² Daniel Rosenmann,² David Czaplewski,²
Jie Gao,^{1,3} and Xiaodong Yang^{1,*}

¹Department of Mechanical and Aerospace Engineering, Missouri University of Science and Technology, Rolla, Missouri 65409, USA

²Center for Nanoscale Materials, Argonne National Laboratory, Argonne, Illinois 60439, USA

³e-mail: gaojie@mst.edu

*Corresponding author: yangxia@mst.edu

Received April 16, 2015; revised May 6, 2015; accepted May 6, 2015;

posted May 8, 2015 (Doc. ID 238097); published May 28, 2015

Broadband perfect absorber based on one ultrathin layer of the refractory metal chromium without structure patterning is proposed and demonstrated. The ideal permittivity of the metal layer for achieving broadband perfect absorption is derived based on the impedance transformation method. Since the permittivity of the refractory metal chromium matches this ideal permittivity well in the visible and near-infrared range, a silica-chromium-silica three-layer absorber is fabricated to demonstrate the broadband perfect absorption. The experimental results under normal incidence show that the absorption is above 90% over the wavelength range of 0.4–1.4 μm , and the measurements under angled incidence within 400–800 nm prove that the absorber is angle-insensitive and polarization-independent. © 2015 Optical Society of America

OCIS codes: (160.3918) Metamaterials; (300.1030) Absorption; (310.4165) Multilayer design; (310.6860) Thin films, optical properties.

<http://dx.doi.org/10.1364/OL.40.002592>

Broadband perfect absorbers in the visible and near-infrared (NIR) range have been widely investigated [1,2] since they are crucial in many promising applications, such as solar energy harvesting [3], thermo-photovoltaic energy conversion [4–6], thermal imaging [7], and emissivity control [8]. Recently, broadband perfect absorbers have been designed according to different mechanisms including multiple resonances [8–11], lattice-scattering effects [12,13], impedance matching [14], and slow-light modes [15–17]. These broadband perfect absorbers have been realized by utilizing metal-dielectric stacks with certain patterned structures, where the noble metal gold is typically used.

In this Letter, a broadband perfect absorber based on one ultrathin layer of the refractory metal chromium (Cr) embedded between two silica (SiO_2) layers without structure patterning is demonstrated. The ideal permittivity of the metal layer for achieving broadband perfect absorption is derived based on the impedance transformation method. Since the permittivity of Cr is close to the ideal metal permittivity in the visible and NIR range compared to other kinds of metals, the demonstrated SiO_2 -Cr- SiO_2 three-layer absorber exhibits absorption higher than 90% over the wavelength range of 0.4–1.4 μm .

Figure 1(a) shows the schematic of the designed absorber consisting of one metal layer (with permittivity ϵ_m and thickness d_m) embedded in two dielectric layers (with permittivity ϵ_d and thickness d_d) on a thick gold substrate (with permittivity ϵ_{Au} and transmission $T = 0$). In order to analyze the absorption A (where $A = 1 - R$ and R is the reflection), the wave impedance is calculated based on the impedance transformation method [18]:

where N_m , n_d , and N_{Au} are the complex refractive indices of the metal layer, the dielectric layer and the gold (Au) substrate, respectively. M and D are the phase shifts in the metal layer and the dielectric layer with $M = \kappa_0 N_m d_m$ and $D = \kappa_0 N_d d_d$ where κ_0 is the wave number in vacuum. The metal layer is ultrathin compared with the optical wavelength so that $\delta_m = \kappa_0 d_m \ll 1$ and $\tan(M) \approx M$. It is also assumed that the real part of the refractive index of the gold substrate is negligible, and it only contains the imaginary part as $N_{\text{Au}} = ik_{\text{Au}}$. The permittivities are defined as $\epsilon_d = n_d^2$ and $\epsilon_m = N_m^2$. Under these conditions, Eq. (1) can be simplified as

$$Z = i \frac{A_1 + A_2 \epsilon_m}{B_1 + B_2 \epsilon_m}, \quad (2)$$

with the real coefficients of A_1 , A_2 , B_1 , and B_2 as functions of $x = \tan(D)$:

$$A_1 = \epsilon_d \tan^2(D) + n_d[-2k_{\text{Au}} + \epsilon_d \delta_m] \tan(D) - \epsilon_d[k_{\text{Au}} \delta_m + 1],$$

$$A_2 = k_{\text{Au}} \delta_m \tan^2(D) + n_d \delta_m \tan(D),$$

$$B_1 = -\epsilon_d[k_{\text{Au}} - \epsilon_d \delta_m] \tan^2(D) - n_d[2\epsilon_d + \epsilon_d k_{\text{Au}} \delta_m] \tan(D) + \epsilon_d k_{\text{Au}},$$

$$B_2 = -n_d k_{\text{Au}} \delta_m \tan(D) - \epsilon_d \delta_m.$$

The complex impedance of $Z = Z' + iZ''$ can be calculated using the given permittivity of the metal layer $\epsilon_m = \epsilon'_m + i\epsilon''_m$.

Eq. (2) implies that the impedance changes periodically as a function of $x = \tan(D)$ when the incident

$$Z = \frac{N_m \tan^2(D)[n_d^2 - iN_{\text{Au}}N_m \tan(M)] + n_d \tan(D)[2iN_{\text{Au}}N_m + (n_d^2 + N_m^2) \tan(M)] - n_d^2[N_m - iN_{\text{Au}} \tan(M)]}{n_d \tan^2(D)[N_{\text{Au}}n_dN_m - in_d^3 \tan(M)] + n_d \tan(D)[2in_d^2N_m + N_{\text{Au}}(n_d^2 + N_m^2) \tan(M)] + n_d^2N_m[-N_{\text{Au}} + iN_m \tan(M)]}, \quad (1)$$

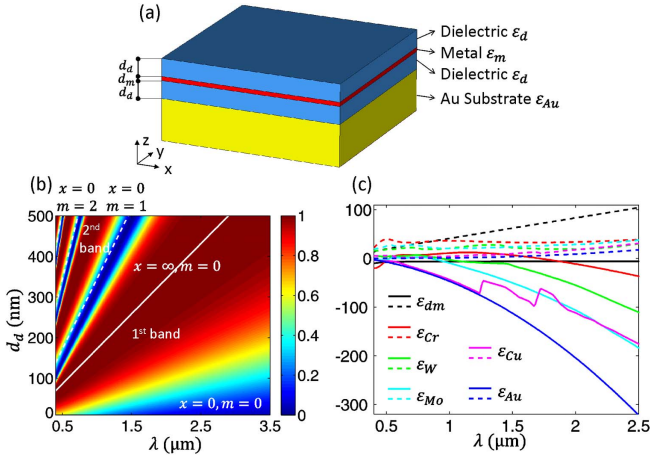


Fig. 1. (a) Schematic of the broadband perfect absorber consisting of one metal layer embedded between two dielectric layers on a gold substrate. (b) The calculated absorption bands of the absorber based on the designed ideal permittivity of the metal layer ϵ_{dm} in Eq. (4) as the function of wavelength λ and SiO_2 thickness d_d , where the thickness of the metal layer is fixed at 8 nm. The white dashed line and the white solid line represent the beginning location and the middle position of each absorption band where $x = 0$ and $x = \infty$, respectively. The first band is between $m = 0$ and $m = 1$. (c) The real (solid curves) and imaginary (dashed curves) parts of the ideal permittivity of the metal layer compared to several other different kinds of metals.

wavelength λ or the thickness of dielectric layer d_d varies. As a result, the absorption will also be altered periodically with λ and d_d , giving rise to different absorption bands. Figure 1(b) shows the calculated absorption bands as a function of the wavelength λ and the thickness of SiO_2 dielectric layer d_d , where the thickness of metal layer is 8 nm and the ideal permittivity of the metal layer, ϵ_{dm} , derived next is considered. Specifically, the beginning location (white dashed line) and the middle position (white solid line) of each absorption band are determined by $x = 0$ and $x = \infty$, respectively, and the corresponding dielectric thickness can be calculated as

$$x = 0: d_d = \frac{m}{2n_d} \lambda_0, \quad m = 0, 1, 2, \dots;$$

$$x = \infty: d_d = \frac{(m + 0.5)}{2n_d} \lambda_0, \quad m = 0, 1, 2, \dots \quad (3)$$

The bandwidth of each absorption band is determined by the ratio between λ and d_d , which is relevant to n_d and the band order m . For the first absorption band, with $m = 0$, when n_d becomes smaller, the absorption wavelength range gets broader. As a result, SiO_2 is selected for the dielectric layer due to its low refractive index ($n_{\text{SiO}_2} = 1.45$). The ideal permittivity of the metal layer ϵ_{dm} is designed to achieve the broadband perfect absorption. It can be shown that at the beginning location of each absorption band ($x = 0$), the absorption is always close to zero since the impedance is $Z \rightarrow 0 - i/k_{\text{Au}}$ as long as the thickness of the metal layer is much smaller than the wavelength, thus obtaining a very high reflection. On the other hand, in order to achieve broadband perfect absorption, the impedance at the middle position

of each absorption band ($x = \infty$) should match the free-space impedance, $Z = Z_0 = 1 + i0$. Then the ideal permittivity of the metal layer as a function of wavelength can be derived as

$$\epsilon'_{dm}(\lambda) = -\frac{\epsilon_d}{k_{\text{Au}} \delta_m}, \quad \epsilon''_{dm}(\lambda) = \frac{\epsilon_d (k_{\text{Au}} - \epsilon_d \delta_m)}{k_{\text{Au}} \delta_m} \quad (4)$$

and is plotted in Fig. 1(c). The permittivities of several different kinds of metals including Cr, tungsten (W), molybdenum (Mo), copper (Cu), and gold (Au) are also plotted for comparison. It is noticed that the permittivity of Cr [19–21] is the closest to the ideal permittivity, while the permittivity of Au [19] is far away from that. Therefore, Cr is selected as the ideal material for the ultrathin metal layer inside the absorber.

The SiO_2 -Cr- SiO_2 three-layer absorber consisting of one 8-nm Cr layer embedded between two 85-nm SiO_2 layers is fabricated on top of a silicon wafer coated with 200-nm-thick gold substrate by DC sputtering. The three layers of the absorber are grown by RF sputtering at a deposition rate of 0.14 $\text{\AA}/\text{s}$ for SiO_2 and 0.5 $\text{\AA}/\text{s}$ for Cr. Figure 2(a) shows a scanning electron microscope (SEM) image of the fabricated absorber where each layer can be clearly seen. The thick gold substrate acts as a mirror to block any transmission through the sample. The black curve in Fig. 2(b) shows the measured absorption spectrum from the fabricated absorber at normal incidence by measuring the reflection using a visible spectrometer together with a FTIR. As expected, high absorption of more than 90% can be obtained over a broad wavelength range from 0.4 μm to approximately 1.4 μm , since the permittivity of Cr is very close to the ideal permittivity of the metal layer to 1.4 μm as shown in Fig. 1(c). Figure 2(b) also plots the calculated absorption spectra for absorbers made of different kinds of metals, including Cr, W, Mo, Cu, and Au, where the absorption spectra from W and Mo are not as broad as from Cr, while the absorption spectra from Cu and Au are quite low.

The calculated absorption as a function of the incident wavelength and the SiO_2 thickness for the designed SiO_2 -Cr- SiO_2 three-layer absorber when the Cr layer thickness is 8 nm is plotted in Fig. 3(a). It is notable that the absorption bands show similar trends as the absorber using the ideal permittivity of metal shown in Fig. 1(b).

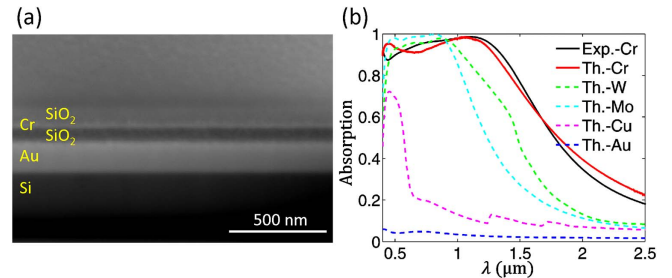


Fig. 2. (a) A cross-section SEM image of the fabricated SiO_2 -Cr- SiO_2 three-layer absorber on a gold substrate. (b) The measured absorption spectrum of the fabricated absorber (black curve) and the simulated absorption spectra from absorbers made of different kinds of metals, including Cr, W, Mo, Cu, and Au.

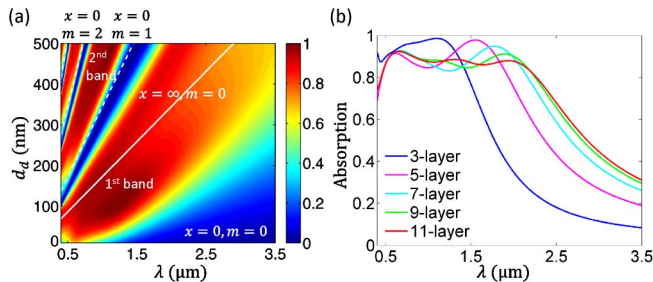


Fig. 3. (a) The calculated absorption of the designed SiO₂-Cr-SiO₂ three-layer absorber as a function of wavelength λ and dielectric thickness d_d when the Cr layer thickness is 8 nm. (b) Absorption spectra under normal incidence for the Cr-SiO₂ absorbers with different numbers of layers.

However, when the wavelength is above 1.4 μm , the absorption will decrease since the permittivity of Cr does not follow the ideal permittivity for longer wavelengths. Moreover, different from the optimal thickness for a single thin metal layer to get the highest absorption [22,23], in the designed SiO₂-Cr-SiO₂ three-layer absorber, the impedance-matching condition is achieved mainly by tuning the thickness of SiO₂ layer, and the approximation of $\tan(M) \approx M$ is satisfied due to $\delta_m = \kappa_0 d_m \ll 1$ for the ultrathin Cr layer. Here the Cr layer thickness is designed as 8 nm by considering the fabrication capability to deposit high-quality thin Cr layer as well as the absorption amplitude and range. In addition, the absorption can be further improved by adding more Cr-SiO₂ layers. As shown in Fig. 3(b), absorption higher than 80% can be reached up to the wavelength of 2.3 μm when the layer number is above 7.

Furthermore, the electric field distribution E_x under normal incidence at the wavelength of 500 nm is plotted in Fig. 4(a) to show the impedance matching for the absorber, where the wavefront propagation inside the absorber remains the same shape as the incident wave in air so that there is no reflection from the absorber. Then the absorption loss of the Cr layer will induce the perfect absorption of the incident light. This is illustrated from the time-averaged power flow \vec{P} [arrows in Figs. 4(a) and 4(b)], which keeps the same optical intensity in the air and in the top SiO₂ layer but decays fast

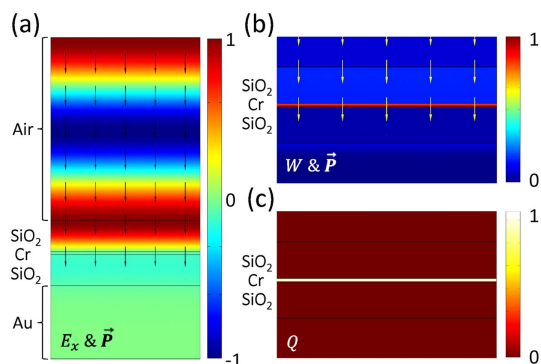


Fig. 4. (a) The calculated electric field distribution E_x and time-averaged power flow \vec{P} (arrows); (b) time-averaged energy density distribution W and power flow \vec{P} ; and (c) heat-generation density distribution Q under normal incidence at the wavelength of 500 nm.

below the Cr layer. Since the time-averaged energy density W is mainly confined inside the Cr layer as shown in Fig. 4(b), the heat generation density distribution Q is mostly located inside the Cr layer rather than the gold substrate as shown in Fig. 4(c). It shows that the gold substrate just acts as a mirror to reflect light back to the Cr layer.

The reflection spectra at different incident angles are measured with a white-light source and a visible spectrometer over a wide spectral range from 400 nm to 800 nm at angles of 15–80 degrees. In Fig. 5, the experimental absorption spectra at different incident angles are reported as well as the calculated results for comparison for both TE and TM polarizations. It is shown that the experimental absorption spectra are in agreement with

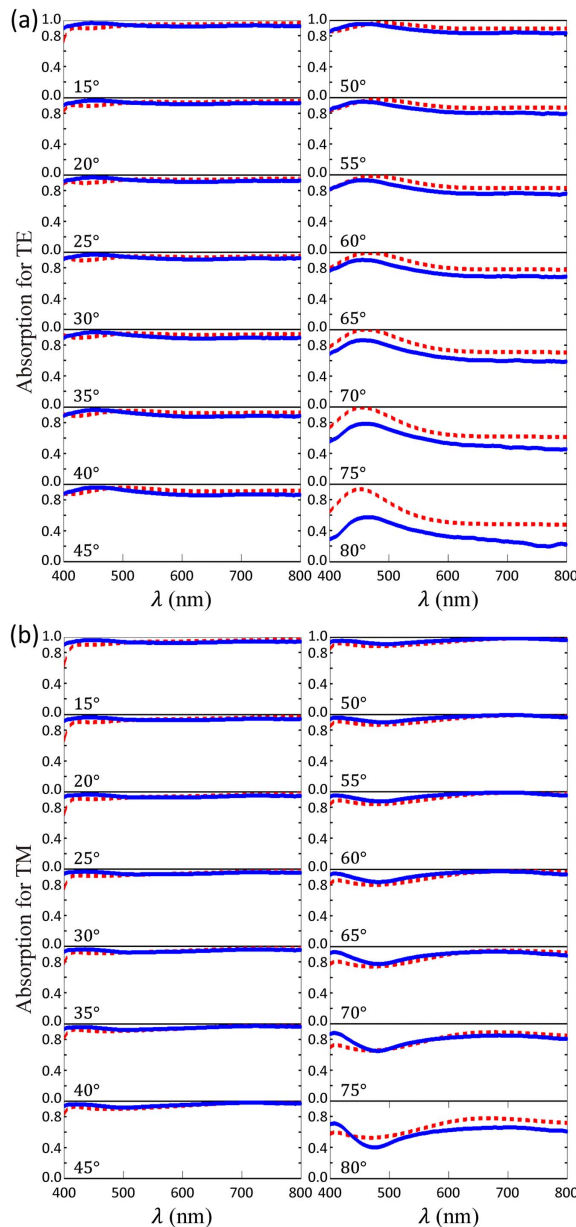


Fig. 5. Measured (solid blue) and calculated (dashed red) absorption spectra in the wavelength range of 400–800 nm at different incident angles (15–80 degrees) for (a) TE polarization and (b) TM polarization.

the theoretical ones except at very high angles close to 80 degrees. The absorption spectra for TE and TM polarizations are the same under normal incidence and similar at low incident angles, but become different at high incident angles above 50 degrees. It is demonstrated that the broadband perfect absorber is incident angle-insensitive and polarization-independent.

Finally, since refractory metals are extraordinarily resistant to heat and with high melting points, the proposed perfect absorbers made of the refractory metal Cr can also act as thermal emitters working at high temperature. For instance, the melting point of bulk Cr is 2180 K where the blackbody radiation has a peak wavelength of 1.33 μm . However, the melting point of bulk Au is just 1337 K leading to a peak wavelength of 2.17 μm for the blackbody radiation. Although the melting points for metals at the nanoscale will be below their bulk values due to size effects [24], refractory metals still hold higher melting points than noble metals. Therefore, emitters made of refractory metals can work at high temperatures to emit light in the visible and NIR range.

In conclusion, a broadband perfect absorber made of the refractory metal Cr without structure patterning is demonstrated. The broadband absorption is analyzed based on the impedance transformation method and the ideal permittivity of the metal layer is derived to design the three-layer absorber. Since the permittivity of the refractory metal Cr is closest to the ideal permittivity of metal in the visible and NIR range, the $\text{SiO}_2\text{-Cr-SiO}_2$ three-layer absorber is fabricated for the demonstration of broadband perfect absorption over the wavelength range of 0.4–1.4 μm . The absorption spectra are also measured at different incident angles with both TE and TM polarizations within 400–800 nm to show the angle-insensitive and polarization-independent properties. The demonstrated broadband absorber based on one ultrathin layer of refractory metal can be used in many exciting applications, such as solar energy harvesting, thermo-photovoltaic energy conversion, thermal imaging, and emissivity control.

The authors acknowledge the support from the Ralph E. Powe Junior Faculty Enhancement Award and the National Science Foundation under grant CBET-1402743. This work was performed, in part, at the Center for Nanoscale Materials, a U.S. Department of Energy, Office of Science, Office of Basic Energy

Sciences User Facility under Contract No. DE-AC02-06CH11357.

[†]These authors contributed equally to this work.

References

1. Y. Cui, Y. He, Y. Jin, F. Ding, L. Yang, Y. Ye, S. Zhong, Y. Lin, and S. He, *Laser Photon. Rev.* **8**, 495 (2014).
2. C. M. Watts, X. Liu, and W. J. Padilla, *Adv. Mater.* **24**, OP98 (2012).
3. T. V. Teperik, F. J. Garcia de Abajo, A. G. Borisov, M. Abdelsalam, P. N. Bartlett, Y. Sugawara, and J. J. Baumberg, *Nat. Photonics* **2**, 299 (2008).
4. S. Molesky, C. J. Dewalt, and Z. Jacob, *Opt. Express* **21**, A96 (2013).
5. C. Wu, B. Neuner III, J. John, A. Milder, B. Zollars, S. Savoy, and G. Shvets, *J. Opt.* **14**, 024005 (2012).
6. H. Deng, T. Wang, J. Gao, and X. Yang, *J. Opt.* **16**, 035102 (2014).
7. N. I. Landy, C. M. Bingham, T. Tyler, N. Jokerst, D. R. Smith, and W. J. Padilla, *Phys. Rev. B* **79**, 125104 (2009).
8. X. Liu, T. Tyler, T. Starr, A. F. Starr, N. M. Jokerst, and W. J. Padilla, *Phys. Rev. Lett.* **107**, 045901 (2011).
9. B. J. Lee and Z. M. Zhang, *J. Appl. Phys.* **100**, 063529 (2006).
10. K. Aydin, V. E. Ferry, R. M. Briggs, and H. A. Atwater, *Nat. Commun.* **2**, 517 (2011).
11. Y. Q. Ye, Y. Jin, and S. He, *J. Opt. Soc. Am. B* **27**, 498 (2010).
12. W. Wang, Y. Cui, Y. He, Y. Hao, Y. Lin, X. Tian, T. Ji, and S. He, *Opt. Lett.* **39**, 331 (2014).
13. J. Yu, Y. Shen, X. Liu, R. Fu, J. Zi, and Z. Zhu, *J. Phys.* **16**, L51 (2004).
14. N. Mattiucci, M. J. Bloemer, N. Akozbek, and G. D'Aguanno, *Sci. Rep.* **3**, 3203 (2013).
15. Y. Cui, K. H. Fung, J. Xu, H. Ma, Y. Jin, S. He, and N. X. Fang, *Nano Lett.* **12**, 1443 (2012).
16. J. Zhou, A. F. Kaplan, L. Chen, and L. J. Guo, *ACS Photonics* **1**, 618 (2014).
17. D. Ji, H. Song, X. Zeng, H. Hu, K. Liu, N. Zhang, and Q. Gan, *Sci. Rep.* **4**, 4498 (2014).
18. H. A. Haus, *Waves and Fields in Optoelectronics* (Prentice-Hall, 1984).
19. E. D. Palik, *Handbook of Optical Constants of Solids* (Academic, 1998).
20. D. Barchiesi and T. Grosgees, *J. Nanophoton.* **8**, 083097 (2014).
21. A. D. Rakic, A. B. Djurišić, J. M. Elazar, and M. L. Majewski, *Appl. Opt.* **37**, 5271 (1998).
22. W. Woltersdorff, *Z. Phys.* **91**, 230 (1934).
23. S.-A. Biehs, D. Reddig, and M. Holthaus, *Eur. Phys. J. B* **55**, 237 (2007).
24. P. Buffat and J. P. Borel, *Phys. Rev. A* **13**, 2287 (1976).